

Enhanced loading of a magneto-optic trap from an atomic beam

Brian P. Anderson and Mark A. Kasevich

Department of Physics, Stanford University, Stanford, California 94305

(Received 7 March 1994; revised manuscript received 26 May 1994)

We demonstrate enhanced loading of a ^7Li magneto-optic trap by broadening the frequency spectrum of the laser trapping light with a resonant electro-optic modulator. We achieve an ~ 20 -fold improvement in the loading rate over that obtained without a broadened spectrum when directly capturing atoms from a divergent atomic beam.

PACS number(s): 32.80.Pj

Efficient capture of atoms from a thermal atomic source is the first step in many laser cooling schemes [1,2] and is of paramount importance for experiments relying on laser-cooled and trapped atomic sources. Examples of such experiments include current efforts aimed at observation of quantum many-body effects in dilute atomic vapors [3], laser-cooled atomic time standards [4,5], and precision atom interferometry experiments [6,7].

Currently employed methods for capture fall into two classes. In the first class, a thermal atomic beam is slowed by a counterpropagating laser beam [8]. In order to ensure that the laser light remains resonant with the Doppler-shifted atomic transition as the atom decelerates, either the frequency of the light is altered (with a frequency chirp [9] or a white-light laser source [10]), or an external field (magnetic [11] or electric [12]) gradient is applied to shift the atomic transition into resonance with the light. In the second class, the low-velocity tail of the Maxwell-Boltzmann distribution is directly captured from a thermal atomic source [13,14].

In the approach described below for ^7Li , atoms in the low-velocity tail of the Maxwell-Boltzmann distribution are captured and loaded directly from an atomic beam into a magneto-optic trap. We achieve high loading rates by (i) minimizing the distance between the atomic oven nozzle and the trapping region and (ii) broadening the frequency spectrum of the trapping light. This method is closely related to the white-light scheme of Ref. [10].

Loading rates that are comparable to those obtained by other methods may also be achieved by locating the nozzle of an atomic-beam oven close to the trapping region [15]. Although traditional methods efficiently reduce the speed of atoms along the propagation axis of the slowing light, they do so at the expense of increasing the divergence (transverse spreading) of the atomic beam. Placing the nozzle close to the trap, on the other hand, reduces losses due to transverse spreading while curtailing the potential effectiveness of longitudinal slowing. An analysis similar to that for a vapor-cell loaded trap [13] predicts a loading rate $R \approx C v_c^4 d^2 / l^2$. Here, C is a constant, v_c is the maximum atomic velocity which can be captured by the trap, d is the diameter of the trapping beams, and l is the distance from the oven nozzle to the trap center. This expression is strictly valid when $d \ll l$ and $v_c \ll \sqrt{k_B T / m}$. The geometric factor of d^2 / l^2 accounts for the spatial localization of the atomic source. As $l \rightarrow d$, the loading rate becomes comparable with the optimal rates obtained using field-gradient slowing techniques.

Our experimental geometry is shown in Fig. 1. The oven nozzle was set back $l \sim 20$ cm from the trap center and d was ~ 1 cm. An atomic-beam shield was located ~ 6 cm from the center of the trapping region between the oven nozzle and the trap center. The shield was mounted on a continuously adjustable stage, which allowed it to be translated from a position that completely blocked the atomic beam to one that fully transmitted the beam. This permitted the shield to be adjusted to a mid-range position where it blocked fast atoms from direct collision with trapped atoms (which typically accumulated in a $200\text{--}500\text{-}\mu\text{m}$ -diam ball near the center of the trapping beams, while sacrificing a factor of ~ 2 in loading rate.

There are at least two important differences between the above geometry and a vapor cell-loaded trap [13]. First, the vapor cell geometry requires the entire vacuum apparatus to be heated to a temperature high enough to yield a partial vapor pressure higher than the background gas pressure. This is awkward for elements like Li, where, for example, this temperature is $\sim 200\text{--}300^\circ\text{C}$. Second, the localization of the atomic source in the beam geometry permits the trap to be shielded from direct collisional impact from high-velocity atoms originating from the source.

The trap capture velocity plays an important role in determining the net loading efficiency. We estimate the capture velocity with the following trap model [16], which we invoke in order to provide a means to assess the relative gains achieved with spectrally broadened trapping lasers. An atom of initial velocity v will be captured if, during its flight through the trapping beams, its velocity is reduced to $v = 0$

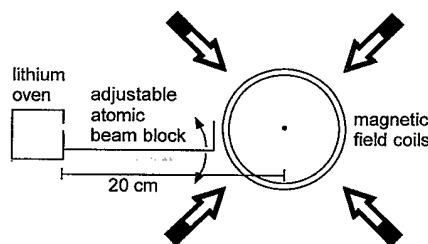


FIG. 1. A schematic illustration of the apparatus. Atoms are loaded directly from the oven into the magneto-optic trap without a precooling (slowing) stage. Laser trapping beams are taken to lie along the (1,0,0), (0,1,0), and (0,0,1) axes, and the oven is located along the (1,1,1) axis.

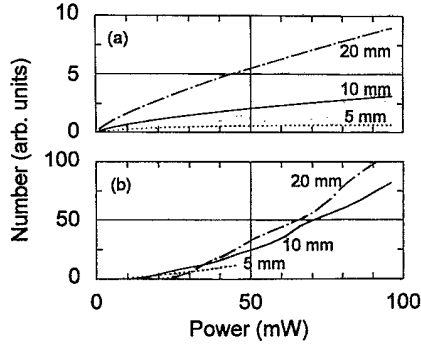


FIG. 2. (a) Modeled loading rate as a function of laser power and beam diameter for single-frequency loading. (b) Loading rate as a function of laser power and beam diameter for comb loading. In both cases, power specifies the total laser power in three beams. A saturation intensity of 5.2 mW/cm^2 was used for these plots.

by the scattering force. For simplicity, we treat the atom as a two-level system in counterpropagating light fields. We approximate the scattering force as

$$\mathbf{f}_s \approx \frac{\hbar \mathbf{k}_{\text{eff}}}{2\tau} \left\{ \frac{S(\mathbf{x})}{1 + S(\mathbf{x}) + 4(\Delta_+ / \gamma)^2} - \frac{S(\mathbf{x})}{1 + S(\mathbf{x}) + 4(\Delta_- / \lambda)^2} \right\}, \quad (1)$$

where $\Delta_{\pm} = \Delta_0 \pm \mathbf{k}_{\text{eff}} \cdot \mathbf{v}$ is the Doppler-shifted detuning (Δ_0 is the detuning of the laser frequency from the atomic resonance and \mathbf{k}_{eff} is the effective propagation vector for the light field), $S(\mathbf{x}) = I(\mathbf{x})/I_{\text{sat}}$ is the ratio of the laser intensity at position \mathbf{x} to the saturation intensity of the atomic transition, and γ is the natural linewidth of the transition. In our experiment the propagation axes of the trapping beams lie along the (1,0,0), (0,1,0), and (0,0,1) axes, while the mean atomic velocity is along the (1,1,1) axis to a good approximation. We incorporate this geometry into a one-dimensional model by combining each beam's contribution to the net scattering force into a mean force acting parallel and another acting antiparallel to the mean atomic flight path. This amounts to taking $|\mathbf{k}_{\text{eff}}| \sim k/\sqrt{3}$. In making the above approximation, we neglect polarization gradient-type forces and stimulated forces. Furthermore, we neglect the Zeeman shifts due to the presence of the magnetic fields. To find the capture velocity we integrate the one-dimensional classical equation of motion using the force law specified in Eq. (1).

Two experimentally adjustable parameters significantly influence the magnitude of the capture velocity v_c : laser beam power and laser beam diameter. Using the model described above, we have numerically explored these dependencies within experimentally accessible limits of laser beam power and diameter. These results are summarized in Fig. 2(a), where we calculate loading rate R as a function of beam diameter and power. In obtaining R we have approximated the trapping light fields as being confined to a cube of volume d^3 oriented with the entrance face perpendicular to the mean atomic velocity, and have taken a flat-top intensity distribution for the laser beams [17]. Figure 3(a) illustrates the velocity dependence of the slowing force.

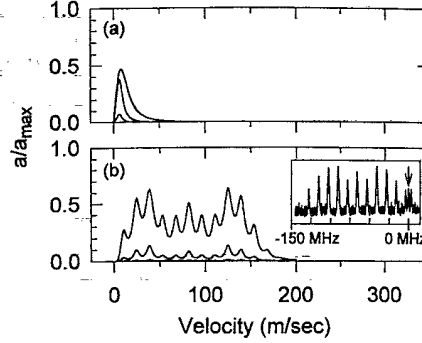


FIG. 3. Calculation of acceleration vs velocity for various laser beam powers for (a) single-frequency loading and (b) comb loading for $I/I_{\text{sat}} = 0.1, 1, \text{ and } 10$ (I is the combined intensity for three laser beams). For our geometry, $a_{\text{max}} = \hbar k_{\text{eff}} / 2m\tau$. The inset shows the optical heterodyne between the comb beam and 816-MHz repumping sideband of the single-frequency trapping beam. The comb parameters (modulation index and sideband separation) are those used to obtain the curves shown in Fig. 2(b). The arrow corresponds to the relative frequency of the -5.5 -MHz detuned single-frequency trapping beams.

Our magneto-optic trap was of the standard design [18]. Two anti-Helmholtz coils generated a magnetic-field gradient of 6 G/cm along the symmetry axis of the coils. The base pressure of the vacuum system was typically 2×10^{-9} torr at an oven temperature of 380°C [19]. The 671-nm output of a dye laser was frequency stabilized to the ${}^7\text{Li } 2S_{1/2}, F=2 \rightarrow 2P_{3/2}, F=3$ optical resonance with a saturated absorption locking technique. A resonant electro-optic modulator, driven at 816 MHz, was used to generate a repumping sideband resonant with the $2S_{1/2}, F=1 \rightarrow 2P_{3/2}$ transitions. The first-order sidebands each had 30% of the power of the carrier. The $1/e^2$ laser beam diameter was fixed at 1.1 cm and its frequency was detuned $-5.5 \pm 0.5 \text{ MHz}$ from the $2S_{1/2}, F=2 \rightarrow 2P_{3/2}, F=3$ resonance (the natural linewidth for this transition is 5.8 MHz). To measure the number of atoms we first simultaneously turned off the trapping beams and the magnetic field after a preset loading interval, then waited 2 msec before pulsing on the trapping beams at 40 mW/cm^2 intensity [20]. (In this and subsequent references to measured intensity or power, we refer to the intensity or power of the carrier plus both of the 816-MHz sidebands.) We determined the number of atoms from the integrated fluorescence imaged onto a charge-coupled-device (CCD) array during a $100\text{-}\mu\text{sec}$ exposure.

Our measurements of the loading rate as a function of beam power, shown in Fig. 4(a), are in good agreement with power scaling predicted by the model presented above. The loading rate was determined by taking the ratio of the number of atoms loaded into the trap to the loading time, in a regime where the number loaded was linear with loading time.

Further gains are possible by spectrally tailoring the laser trapping light. An increase in spectral width increases the capture velocity by allowing the laser light to efficiently couple to the Doppler-shifted resonances of faster atoms. For our experiment we used an electro-optic modulator to broaden our light source. The electro-optic modulator was

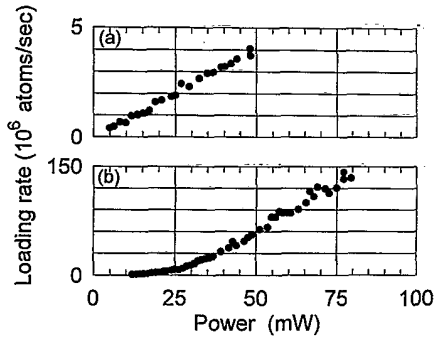


FIG. 4. Observed loading rates for (a) single-frequency loading and (b) comb loading. Power refers to the total laser power in three beams.

resonantly driven at 12.5 MHz to produce a comb of sidebands, ranging nominally in frequency from 134 MHz (minus fifth order) to 9 MHz (plus fifth order) below the $2S_{1/2}, F=2 \rightarrow 2P_{3/2}, F=3$ transition.

We incorporate the comb into our model for loading efficiency by modifying the expression for the scattering force to reflect the presence of the additional spectral components in the radiation field. In the low-intensity limit each sideband contributes a force component given by Eq. (1), yielding a net force

$$\mathbf{f}_{\text{comb}} \approx \frac{\hbar \mathbf{k}_{\text{eff}}}{2\tau} \sum_i \left\{ \frac{S_i(\mathbf{x})}{1 + S_i(\mathbf{x}) + 4(\Delta_{-,i}/\gamma)^2} - \frac{S_i(\mathbf{x})}{1 + S_i(\mathbf{x}) + 4(\Delta_{+,i}/\gamma)^2} \right\}, \quad (2)$$

where the index i ranges over the sidebands in the comb, $S_i(\mathbf{x})$ is the saturation parameter associated with the intensity in the i th sideband, and $\Delta_{\pm,i} = \Delta_{0,i} \pm \mathbf{k}_{\text{eff}} \cdot \mathbf{v}$ is the Doppler-shifted detuning of the i th sideband. Figure 3(b) shows a plot of Eq. (2) for the frequency parameters used in our experiment at various laser beam powers. The resulting loading rates are shown in Fig. 2(b).

Experimentally we infer as much as a factor of 22 improvement in loading rate over the maximum rate observed with single-frequency loading [21]. For these observations a second beam of 1.3 cm $1/e^2$ diameter, with the comb frequency spectrum described above, was made to copropagate with the original single-frequency trapping beams. The six single-frequency beams were detuned from resonance by -5.5 MHz and each had a peak intensity of $100 \mu\text{W}/\text{cm}^2$. The observed loading rate, shown in Fig. 4(b) as a function of total power in three (of six) comb beams, is in good agreement with the simple models. These models predict a factor of ~ 17 improvement for 64-mW power and a 1-cm beam diameter. (For comparison with theory, the measured powers need to be scaled to account for the fraction of power in the nonresonant 816-MHz sideband. In this case 64 mW is the power in the carrier and the resonant repumping sideband corresponding to the measured 80-mW total power.) Extrapolating our single-frequency loading data in Fig. 4(a) to 80 mW power (neglecting the predicted saturation in loading rate), we infer a factor of 22 improvement. We characterized

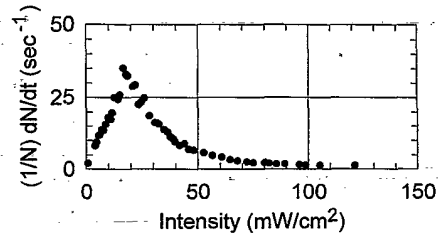


FIG. 5. Normalized trap loss rate $(1/N)dN/dt$ as a function of total trap intensity (i.e., the combined intensity for six trapping beams). The loss rate was measured in a ~ 10 -msec interval just following the extinction of the comb beam.

the frequency spectrum of the comb with an optical heterodyne between the comb beam and an unmodulated reference beam [see inset of Fig. 3(b)].

The use of two sets of beams gave us independent control over the trap loading parameters, determined to a large extent by the comb beams, and the trap cooling parameters, which were set by the single-frequency beams. With two sets of beams, for example, we were able to load the trap with both sets on, then turn the comb beams off, leaving the single-frequency beams to cool and compress the loaded atoms.

The number of atoms loaded into the trap after a fixed time depends not only on the loading rate, but also on the rate at which atoms are ejected from the trap. Three important collision-induced ejection mechanisms are background gas collisions with thermal atoms, fine-structure changing collisions, and radiative escape collisions [22]. The net ejection rate depends on the collision rate pertinent to each mechanism, the kinetics of the collision mechanism, and on the depth of the trap. It has recently been noted that the fine-structure ejection mechanism for lithium traps can be suppressed for sufficiently deep traps [23,24]. In the fine-structure changing collision, $\text{Li}(2S_{1/2}) + \text{Li}^*(2P_{3/2}) \rightarrow \text{Li}(2S_{1/2}) + \text{Li}^*(2P_{1/2}) + \Delta E_{\text{FS}}$. The resulting kinetic energy ΔE_{FS} corresponds to a final velocity of $v_{\text{FS}} = 24$ m/sec for each interacting atom (the atoms are nearly at rest before the collision), which can be smaller than the capture velocity of the magneto-optic trap. Thus the collision products may be recaptured. The situation is different for the heavier alkali metals such as Cs and Rb, where the fine-structure splitting is much greater than the 10-GHz interval of Li.

We have experimentally characterized the collision-induced loss processes by observing the decay in the number of trapped atoms as a function of trap depth. We varied trap depth by changing the intensity of the trapping beams. For these measurements, we first loaded the trap with the comb on and a fixed intensity for the single-frequency trapping beams. After loading $\sim 6 \times 10^7$ atoms into the trap, the comb beams were turned off and the single-frequency trapping intensity was switched to the level for the decay measurement. By monitoring the decay in fluorescence, we extracted the normalized number loss rate, $(1/N)dN/dt$ (N is the number of trapped atoms), for the time interval immediately following the extinction of the comb beams. At low intensities, the loss rate increases linearly with intensity and the number of trapped atoms in the $2P_{3/2}$ state, as shown in Fig. 5. At higher intensities the trap becomes sufficiently deep to recap-

ture fine-structure-changing collision products. We can make a crude estimate of trap depth using methods similar to those used above to estimate loading efficiency. In general, the threshold intensity for recapture will depend on the angle of ejection relative to the propagation axes of the trapping beams. If we consider flight along the (1,1,1) axis, we estimate a recapture intensity of ~ 20 mW/cm² for our trap parameters, in reasonable agreement with the data.

The success of the comb-loaded Li trap may hinge on its ability to recapture decay products. In general, the presence of nearly resonant, red-detuned light produces fine-structure changing collisions by inducing transitions to excited molecular states [22]. For Li this collision rate varies only weakly with detuning for the detuning range used to generate the comb light [25]. If the trap were not deep enough to recapture fine-structure collision products, the presence of the comb light might induce a trap loss which could prevent a significant buildup of atoms. These collisions may have been responsible for the failure of earlier efforts to trap with broadband laser sources, where the work was done with heavier alkali metals [16,26]. The comb technique might be used for other species if the central area of the comb beam profile is blocked, thus producing a region where trapped atoms can accumulate without suffering additional comb-

induced losses [27,28]. We note, however, that the excited-state hyperfine structures of the heavier alkali metals are significantly different from Li. Finally, loss rates due to background gas collisions and radiative escape should also be reduced due to the substantial increase in trap depth.

In addition to improving the trap loading rate with the comb scheme, we have also observed improvements in trap density. Under the conditions described above, we have observed densities as high as $2_{-1}^{+2} \times 10^{11}$ atoms/cm³. We determined the density by measuring the absorption of a weak probe beam at several detunings from the $2S_{1/2} \rightarrow 2P_{3/2}$ transition. We checked the density measurement with our CCD imaging system by analyzing the spatial intensity distribution of scattered light during the detection pulse.

In conclusion, we have increased capture efficiency and trap density by frequency modulating the laser trapping beams, and have suggested a likely failure mechanism for earlier experiments along these lines.

This work was supported in part by the NSF. We acknowledge stimulating discussions with E. Riis and T. Walker, and thank T. Gustavson and T. Maurin for their experimental support.

-
- [1] S. Chu *et al.*, Phys. Rev. Lett. **55**, 48 (1985).
 [2] J. Prodan *et al.*, Phys. Rev. Lett. **54**, 992 (1985).
 [3] E. Cornell *et al.*, Phys. Rev. Lett. **67**, 2439 (1991); C. Monroe *et al.*, *ibid.* **70**, 414 (1993).
 [4] K. Gibble and S. Chu, Phys. Rev. Lett. **70**, 1771 (1993).
 [5] A. Clairon *et al.*, Europhys. Lett. **16**, 165 (1991).
 [6] D. Weiss *et al.*, Phys. Rev. Lett. **70**, 2706 (1993).
 [7] M. Kasevich and S. Chu, Phys. Rev. Lett. **67**, 181 (1991).
 [8] For a recent review, see W. D. Phillips in *Laser Manipulation of Atoms and Ions*, Proceedings of the Varenna Summer School, edited by E. Arimondo, W. Phillips and F. Strumia (North-Holland, Amsterdam, 1993), pp. 289–343.
 [9] W. Ertmer *et al.*, Phys. Rev. Lett. **54**, 996 (1985).
 [10] M. Zhu *et al.*, Phys. Rev. Lett. **67**, 46 (1991).
 [11] W. D. Phillips *et al.*, J. Opt. Soc. Am. B **2**, 1751 (1985).
 [12] R. Gaggl *et al.*, Phys. Rev. A **49**, 1119 (1994).
 [13] C. Monroe *et al.*, Phys. Rev. Lett. **65**, 1571 (1990).
 [14] A. Cable *et al.*, Opt. Lett. **15**, 507 (1990).
 [15] See, for example, W. Ketterle and D. Pritchard, in *Fundamentals of Quantum Optics III*, edited by F. Ehlotzky (Springer-Verlag, New York, 1993), pp. 77–89.
 [16] K. Lindquist *et al.*, Phys. Rev. A **46**, 4082 (1992).
 [17] We find the loading rates for Gaussian beam profiles to be comparable to those of flat-top profiles.
 [18] E. Raab *et al.*, Phys. Rev. Lett. **59**, 2631 (1987).
 [19] Recently pressures of $\sim 10^{-10}$ torr have been achieved in vapor-cell-loaded traps (E. Cornell, private communication).
 [20] The 2-msec interval for ballistic expansion allowed simultaneous determination of the trap temperature and number by imaging the spatial profile of the expanding cloud of atoms. The magnetic field switched off in less than 1 msec.
 [21] The operating detuning for the single-frequency beam was that used to optimize temperature and density of trapped atoms. Our model predicts substantial improvements in the single-frequency loading rate at larger detunings. For example, the loading rate at -6.5γ detuning with 64-mW power in three beams of 1 cm diameter is ~ 7 times that for the parameters used to generate Fig. 2(a). However, this improved loading rate would be at the expense of trap temperature and density.
 [22] See, for example, A. Smith *et al.*, Phys. Rev. A **46**, 4091 (1992).
 [23] J. Kawanake *et al.*, Phys. Rev. A **48**, R883 (1993).
 [24] N. Ritchie, E. Abraham, Y. Xiao, and R. Hulet (unpublished).
 [25] R. Hulet (private communication).
 [26] K. Gibble *et al.*, Opt. Lett. **17**, 526 (1992).
 [27] E. Riis (private communication).
 [28] The idea of blocking the central region of the trapping beams to enhance trap performance was first introduced in W. Ketterle *et al.*, Phys. Rev. Lett. **70**, 2253 (1993).